Neuron
Article

Propagation of Tau Pathology in a Model of Early Alzheimer's Disease

Alix de Calignon,[1,2,8] Manuela Polydoro,[1,8] Marc Suárez-Calvet,[1,3] Christopher William,[1] David H. Adamowicz,[1] Kathy J. Kopeikina,[1,4] Rose Pitstick,[5] Naruhiko Sahara,[6] Karen H. Ashe,[7] George A. Carlson,[5] Tara L. Spires-Jones,[1] and Bradley T. Hyman[1,*]

[1]MassGeneral Institute for Neurodegenerative Disease, Department of Neurology, Alzheimer's Disease Research Laboratory, Massachusetts General Hospital, Harvard Medical School, Charlestown, MA 02129, USA
[2]Department of Physiology, Anatomy, and Genetics, University of Oxford, Oxford OX1 3QX, UK
[3]Department of Neurology, Hospital de la Santa Creu i Sant Pau, Universitat Autònoma de Barcelona, Barcelona 08025, Spain
[4]Department of Anatomy and Neurobiology, Boston University School of Medicine, Boston, MA 02118, USA
[5]McLaughlin Research Institute. Great Falls, MT 59405, USA
[6]Department of Neuroscience, Center for Translational Research in Neurodegenerative Disease, University of Florida, Gainsville, FL 32610, USA
[7]Department of Neurology, University of Minnesota Medical School, Minneapolis, MN 55455, USA
[8]These authors contributed equally to this work
*Correspondence: bhyman@partners.org
DOI 10.1016/j.neuron.2011.11.033

SUMMARY

Neurofibrillary tangles advance from layer II of the entorhinal cortex (EC-II) toward limbic and association cortices as Alzheimer's disease evolves. However, the mechanism involved in this hierarchical pattern of disease progression is unknown. We describe a transgenic mouse model in which overexpression of human tau P301L is restricted to EC-II. Tau pathology progresses from EC transgene-expressing neurons to neurons without detectable transgene expression, first to EC neighboring cells, followed by propagation to neurons downstream in the synaptic circuit such as the dentate gyrus, CA fields of the hippocampus, and cingulate cortex. Human tau protein spreads to these regions and coaggregates with endogenous mouse tau. With age, synaptic degeneration occurs in the entorhinal target zone and EC neurons are lost. These data suggest that a sequence of progressive misfolding of tau proteins, circuit-based transfer to new cell populations, and deafferentation induced degeneration are part of a process of tau-induced neurodegeneration.

INTRODUCTION

It has been known for more than 25 years that neurofibrillary tangles have a hierarchical pattern of accumulation reflecting selective vulnerability of neuronal populations in the Alzheimer's disease (AD) brain, initially affecting the large projection neurons that connect memory-related neural systems (Braak and Braak, 1991; Hyman et al., 1984). The first neurons to be affected are in layer II of the entorhinal cortex (EC), the neurons that give rise to the perforant pathway, the single major projection linking the cerebral cortex with the hippocampus (Gómez-Isla et al., 1996; Hyman et al., 1987). Over the years, a "march" of lesions appears to propagate across limbic and association cortices, creating a pattern so consistent as to be incorporated into criteria for the neuropathological diagnosis of the illness (Hyman and Trojanowski, 1997). Selective loss of these neurons is believed to contribute to the defects in memory and higher-order cognitive functions in AD due to disconnection and deafferentation of critical neural circuits (Delacourte et al., 1999; Hyman et al., 1990).

Despite recognition of the patterns of anatomical connectivity that link vulnerable neurons, there is no clear understanding of the mechanism of disease progression. To create a model of the earliest point in the neurodegenerative cascade of AD, we generated a transgenic mouse model in which a mutant form of the microtubule binding protein tau (MAPT) (P301L) linked to tangle formation in frontotemporal dementia is expressed selectively in a fraction of the neurons of layer II of the EC (EC-II).

The EC is the predominant cortical input and output network of the hippocampal formation. These connections are layer specific. The superficial layers provide neuronal projections to the dentate gyrus in a powerful projection referred to as the perforant pathway (Witter, 2007). In the mouse, layer II of the EC projects directly to the outer two-thirds of the molecular layer of the dentate gyrus, where it connects to dendrites from the granule cells of the dentate gyrus (Hjorth-Simonsen and Jeune, 1972; Steward, 1976). The major projection patterns are exquisitely specific, with lateral EC (LEC) projecting to the outer third of the dentate molecular layer and the medial EC projecting to the middle third. Smaller projections provide direct EC-hippocampal and EC cortical connections as well. The superficial layers of EC receive output from pre- and parasubiculum, while the deeper layers—layers IV, V, and VI—receive output from hippocampus (Canto et al., 2008).

With this transgenic mouse model, we tested the hypothesis that tau pathology would evolve in the same predictable pattern as the neuropathological development of AD. The results show

dramatic "spread" of pathological tau deposits from the neurons initially expressing human tau *MAPT* messenger RNA (mRNA) (referred to here as tau or htau mRNA) to populations of neurons without detectable transgene expression, leading to coaggregation of human tau and endogenous mouse tau in neurons without detectable levels of human tau mRNA transgene. These data support the idea that local tau aggregation can be transmitted from neuron to neuron, and may help explain the anatomical patterns of tangle accumulation in AD, supporting the hypothesis that circuit-based patterns of neurodegeneration play an important role in the progression of tau pathology.

RESULTS

Restricted Transgene Expression and Age-Dependent Pathology in the EC of rTgTauEC Mice

We generated a mouse line that reversibly expresses human variant tau P301L primarily in EC-II, the rTgTauEC mouse (Figure 1A). We took advantage of a mouse line in which expression of a tet transactivator transgene is under control of the neuropsin gene promoter (Yasuda and Mayford, 2006). This line was crossed with the Tg(tetO-tau$_{P301L}$)4510 line that only expresses human tau carrying the P301L frontotemporal dementia mutation in the presence of a tet transactivator (Santacruz et al., 2005). Human tau expression in bigenic rTgTauEC mice is limited largely to the superficial layers of medial EC and the closely related pre- and parasubicular cortices (Figures 1B and 1C).

We assessed the expression of the human tau transgene in this model by in situ hybridization. We observed intense expression as early as 3 months of age in a subset of neurons in the medial EC (MEC) and pre- and parasubiculum (Figure 1C). The positive neurons in the MEC were detected prominently in layer II, although rare positive neurons were observed in layer III, especially in the area adjacent to the parasubiculum. A few rare neurons in the granular layer and the hilum of the dentate gyrus (DG) showed some transgene expression in accord with observations in the parental line (Yasuda and Mayford, 2006), as well as very rare neurons in the CA1, CA3, lateral amygdaloid nucleus, and superficial cortical areas.

Immunohistochemistry using the 5A6 antibody (courtesy of Dr. G.V. Johnson, University of Rochester), a monoclonal antibody raised against the longest form of recombinant human tau which recognizes an epitope between amino acids 19 and 46 (Johnson et al., 1997), confirmed strong expression of tau protein in superficial layers of the MEC and parasubiculum in rTgTauEC mice at 3 months of age compared to a control brain (Figure 1D). Higher magnification of the EC and DG area showed transgene expression restricted to the EC, where there is diffuse axonal staining, and to the axonal terminals in the middle molecular layer of DG, which receives axons originating in the MEC. This finding indicates that the human tau is transported through axons of the MEC to their terminals in the molecular layer of DG (Figure 1D, middle panels). Immunohistochemistry and western blot analysis of Tg(tetO-tauP301L) tau mice brains revealed no detectable levels of human tau protein expression (Figures S1A and S1B, respectively, available online). Quantitative PCR (qPCR) revealed <2% of rTgTauEC levels of htau mRNA in the parental tauP301L line without transactivator within the noise of the assay (Figure S1C).

Human tau expression in the MEC results in an age-dependent accumulation of tau pathology in transgene expressing neurons. The normal axonal distribution of human tau (Figure 1D) is lost and the protein accumulates in the EC cell bodies. The first sign of tau pathology was detected at 3 months of age with Alz50 staining, an early indicator of tau misfolding, in the projection input zone of MEC, corresponding to the middle third of the molecular layer of the DG (Figure 1E, left most panel), while the inner and outer layers were nonreactive (for higher magnification, see Figure S2). This axonal staining preceded Alz50 staining in the MEC neuronal soma, where Alz50-positive tau was first detected at 6 months of age (Figure 1E, second left panel). From 6 months, a slow progression of tau epitopes in the soma of MEC neurons toward later stages of pathology was observed, marked by the presence of PHF1 staining, recognizing the late phosphorylation of Ser 396/404 sites, starting at the age of 12 months (Figure 1E, middle panel, and Figure S2), Gallyas staining (Paired Helical Filament-specific silver impregnation) was first noted at the age of 18 months (Figure 1E, second right panel, and Figure S2), and Thioflavin S staining (β-pleated sheet conformation) was detected at the age of 24 months (Figure 1E, right panel, and Figure S2).

Biochemical characterization of mouse brain extracts confirmed age-dependent pathological changes in tau protein in rTgTauEC mice (Figure 2). Western blot analysis of whole brain extracts obtained from 12-, 18-, and 24-month-old rTgTauEC and control mice confirmed human tau protein is expressed in the brain and showed an age-dependent increase in total tau and human tau (Figures 2A–2C). Quantification of tau hyperphosphorylation by western blot analysis of mouse brain extracts from 12-, 18-, and 24-month-old rTgTauEC and control mice was performed using phosphorylated tau antibodies AT180 (pT231), PHF1 (pS396/404), and CP13 (pS202) and normalized to total tau levels (phosphorylation-independent). rTgTauEC mice showed an age-dependent increase in all phosphorylated epitopes (Figures 2D–2F). Twenty-four-month-old mouse brains were subjected to sarkosyl extraction to biochemically confirm the presence of insoluble tau aggregates. After sarkosyl extraction, a 64 kDa insoluble hyperphosphorylated tau species was detected by immunoblotting in both rTg4510 and rTgTauEC brains, but was absent in age-matched control brains when analyzed using a total tau antibody (Figures 2G and 2H). In the soluble fraction, the 55 kDa species of tau were also present, similar to that seen in rTg4510 mice (Santacruz et al., 2005).

Human Tau Protein Propagates to Synaptically Connected Brain Regions

The data above establish that human tau mRNA expression in the MEC results in human tau protein expression and age-dependent pathological accumulation in this region, as would be expected. Restricting the transgene expression to the EC also allowed us to investigate whether pathological tau changes spread through neural circuits as predicted from pathological studies of AD brain at different stages. The major output of the EC is a large axonal projection called the perforant pathway that carries input from EC-II and EC-III to the hippocampus, terminating in the middle molecular layer of the DG (Steward, 1976; Van Hoesen and Pandya, 1975). We hypothesized that

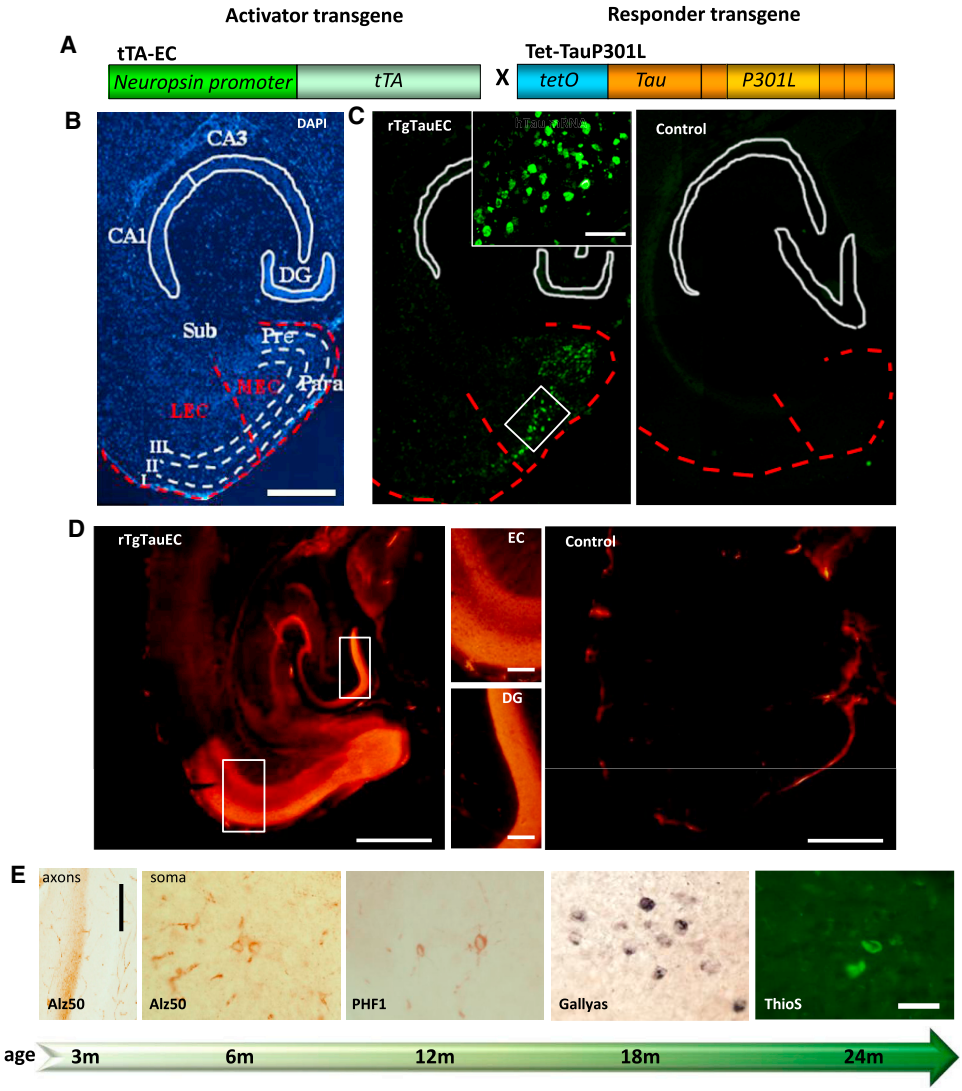

Figure 1. MEC-Restricted Expression of Human P301L-Mutated Tau Causes Progressive Tauopathy in EC Neurons

(A) rTgTauEC transgenic mice express human tau_{P301L} under a tetracycline-responsive promoter (tetO) and the tetracycline transactivator (tTA) under the neuropsin promoter.

(B and C) Low-magnification view of a medial horizontal section of rTgTauEC mouse brain stained with DAPI (B) and FISH showing human tau mRNA (C) demonstrates the restriction of expression of human tau_{P301L} to layer II of the MEC and the pre- and parasubiculum (Pre, Para). The EC and MEC are outlined with a red dotted line. Note the lack of expression in the LEC, the subiculum (Sub), and the hippocampus including the DG, CA3, and CA1. There was no transgene expression in age-matched controls (C, right panel; scale bar, 1 mm). Higher-magnification inset in (C) shows the white outline EC area (scale bar, 100 μm).

(D) Immunohistolabeling with phosphorylation-independent tau antibody 5A6 shows that tau protein is intensely expressed from 3 months of age compared to an age-matched control brain. Scale bar, 1 mm left and right panels, 200 μm in higher-magnification insets (center panels).

(E) Human tau-expressing neurons in the MEC develop progressive tau pathology beginning at 3 months of age, with Alz50-positive tau misfolding in the axon terminal zone (molecular layer of the DG, left panel; scale bar, 200 μm). By 6 months of age, MEC neurons have Alz50-positive tau staining in their soma, and the soma in this region increasingly accumulate pathological forms of tau with age, shown here by markers of later tau pathology including PHF1 (tau phosphorylated at Ser396 and Ser404) starting from 12 months, Gallyas silver stain-positive neurons from 18 months, and Thioflavin S-positive neurofibrillary tangles by 24 months of age. Scale bar, 50 μm for all soma images.

tau expression in the MEC would lead to pathological tau accumulation in a hierarchical fashion, first in the MEC, followed by the DG, then the CA2/3 and CA1 regions, which are downstream of the DG.

To test the possibility that misfolding of tau could be propagated anterogradely along a neural network, areas that are synaptically connected to the EC were investigated with histological stains of tau pathology (Figures 3A–3C; also see Table S1). We find that neurons in the granular layer of the DG developed tau pathology several months after lesions appeared in the MEC, with Alz50-positive and PHF1-positive soma appearing in the DG at 18 months and Gallyas- and Thioflavin S-positive

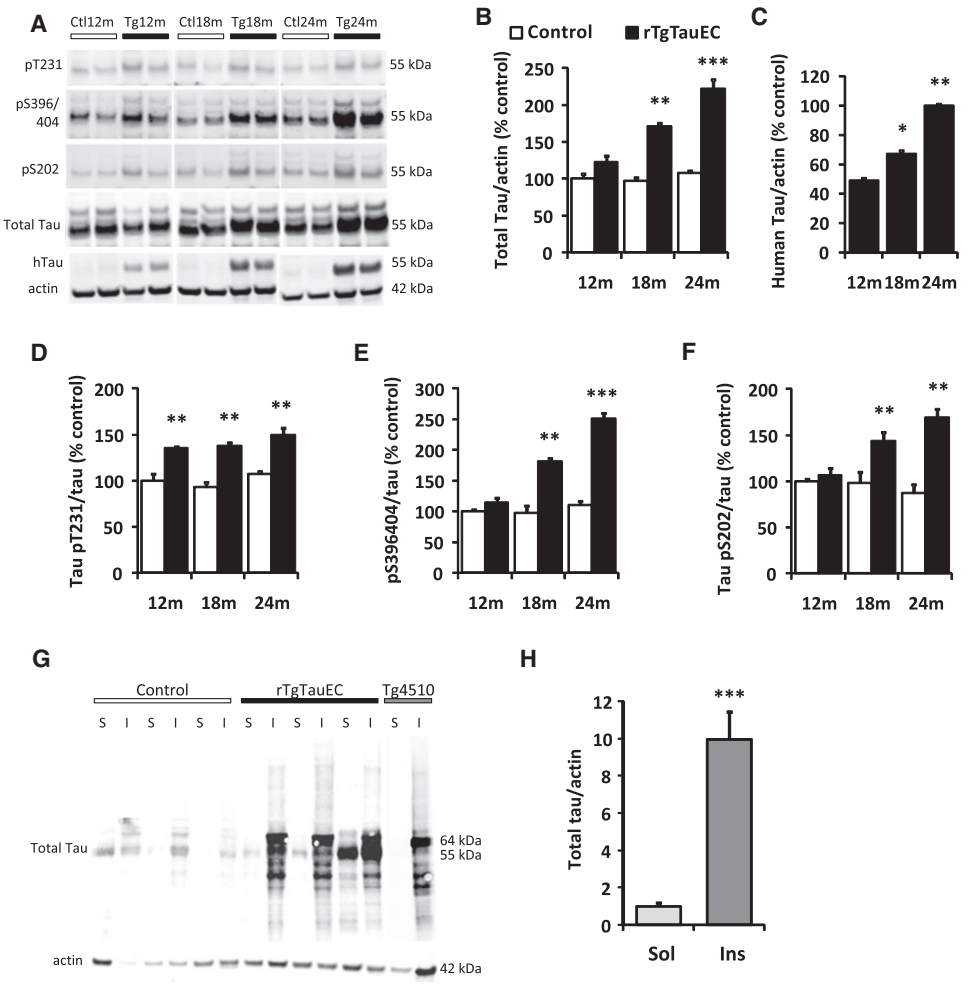

Figure 2. Biochemical Characterization of Tau Pathology Reveals Age-Dependent Increase in Tau Hyperphosphorylation and Presence of Sarkosyl-Insoluble Tau in rTgTauEC

(A–F) Representative immunoblots from western blot analysis of mouse brain extracts from 12-, 18-, and 24-month-old rTgTauEC and control mice. Antibodies specific to phosphorylated tau (AT180 [pT231], PHF1 [pS396/404], and CP13 [pS202]), total tau, and human tau (htau) were used. Quantification of immunoblots shows that rTgTauEC mice present an age-dependent increase in total tau (B), human tau (results are expressed as percent of total tau expression at 24 months, the highest expression point defined as 100%) (C), and phosphorylated epitopes (D–F) (n = 4 mice per group). A series of ultracentrifugation and extraction steps were used to obtain sarkosyl-insoluble fractions of tau from whole brain of 24-month-old rTgTauEC, control (25 μg of protein loaded), and 18-month-old rTg4510 mice (5 μg of protein loaded) (positive control).

(G) Representative western blots of sarkosyl fractions are shown. Sarkosyl soluble (S) and insoluble fractions (I) were immunoblotted with total tau antibody (phosphorylation-independent, Dako). Control mice did not show sarkosyl-insoluble tau. In contrast, immunoblotting of fractions from rTgTauEC mice revealed sarkosyl-insoluble complexes of tau, of the same type as found in the brains of rTg4510 mice. A 64 kDa insoluble hyperphosphorylated tau species was detected by immunoblotting in both rTg4510 and rTgTauEC brains but was absent in age-matched control brains when analyzed using total tau antibody. In the soluble fraction, the 55 kDa species of tau was also present, similar to the species present in rTg4510 mice.

(H) Quantification of samples of sarkosyl fractions (n = 3 mice per group). Results are expressed as the mean ± SEM. *p < 0.05; **p < 0.01; ***p < 0.001.

soma appearing at 24 months (Table S1; Figure S2). CA1 and CA2/3 also develop pathological aggregates by 21 months of age (Figures 3A–3C, middle and right panels). Western blot analysis was used as an alternative approach to address if human tau protein and tau hyperphosphorylation are spread to downstream synaptically connected neurons. The levels of human tau expression and tau phosphorylation were quantified in the EC and hippocampus dissected from 17-month-old rTgTauEC and controls. Human tau protein as well as PHF1 tau could be detected in the EC and hippocampus of rTgTauEC (Figures S3A and S3B), confirming the histological data showing human tau protein present in the hippocampal formation.

This observation of human tau protein and pathology in areas that largely do not express the human tau transgene indicates that tau pathology spreads from cells expressing the transgene to downstream neurons. Indeed, combined fluorescence in situ hybridization (FISH) and immunofluorescent staining for both human tau protein and Alz50 revealed neurons with human tau

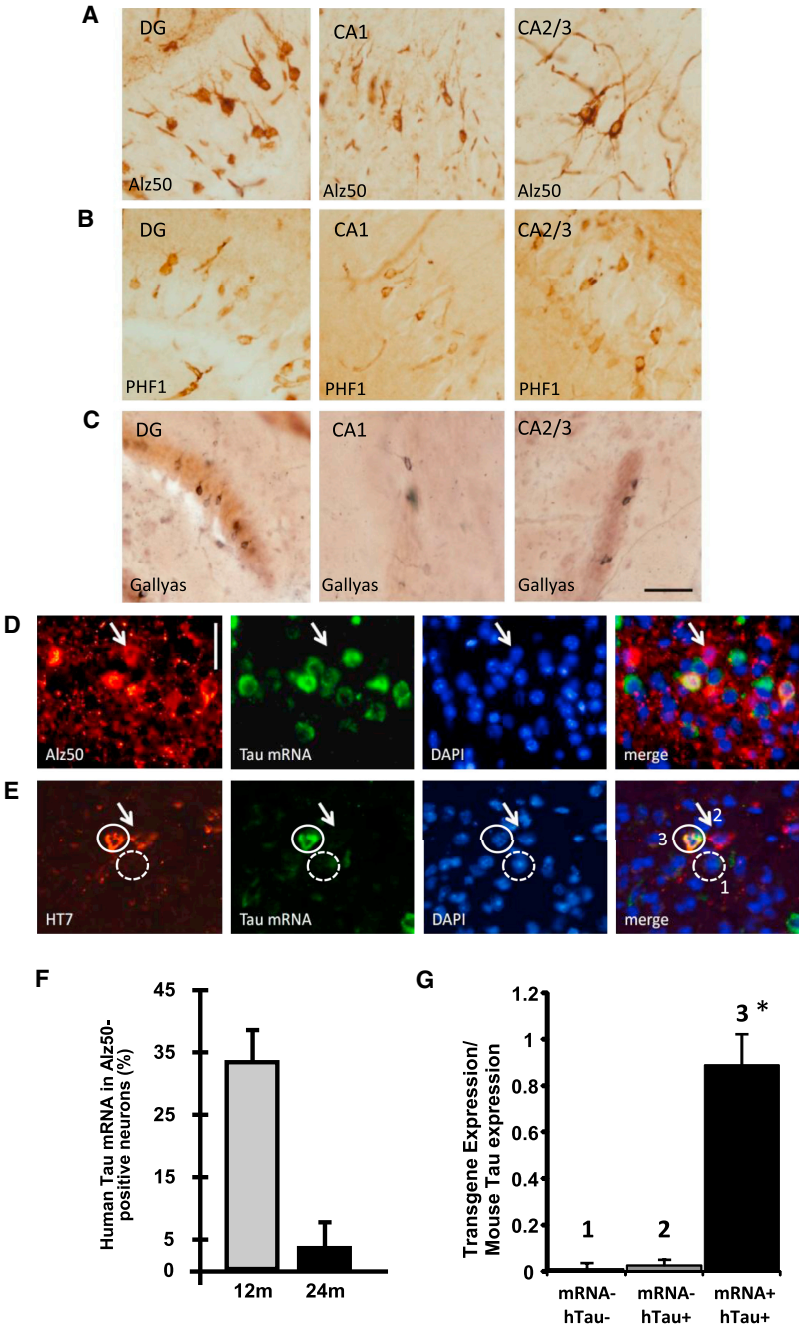

Figure 3. Tau Propagates through Neural Circuits to mRNA-Negative Cells

(A–C) Several markers of pathological tau accumulation: Alz50 (A), PHF1 (B), and Gallyas silver staining (C) appear in brain regions synaptically connected to EC via the perforant pathway, including DG, CA1, and CA2/3 (scale bar, 50 μm).

(D and E) FISH for tau mRNA (green), coupled with immunolabeling (red) with Alz50 (D) or HT7 (E) shows absence of mRNA in some cells containing the tau protein (arrows). Scale bar, 20 μm.

(F) Colocalization of tau mRNA and Alz50-positive aggregates was assessed by stereology at different ages and compared to the total population of neurons carrying Alz50 aggregates. At 12 months of age, a third of the neurons affected by the tau pathology were expressing the transgene, while only ~3% were positive for the MAPT gene at 24 months of age.

(G) FISH for MAPT mRNA [green in (E)] coupled with immunolabeling using HT7 [red in (E)] in the same EC sections from 17-month-old animals was used to laser capture three different populations of cells: (1) tau mRNA-negative and human protein-negative neurons; (2) mRNA-negative and human tau protein-positive neurons; and (3) transgene mRNA-positive and human tau protein-positive neurons. Total RNA was extracted and qPCR analysis of the cDNA product was carried out using primers against the transgenic human tau construct, showing that the neurons that were human tau protein-positive and were RNA-negative by FISH did not express the tau transgene, confirming tau transmission to neurons that do not express the human tau transgene. Results are expressed as the mean ± SEM. *$p < 0.001$.

and/or misfolded tau that do not have detectable levels of human tau transgene in the EC (Figures 3D and 3E), hippocampal fields (Figures S3C and S3D), and anterior cingulate cortex (Figure S3E) showing a dissociation between htau expression and human tau protein accumulation. In the EC, quantification of human tau mRNA and Alz50-positive cells revealed that only 33.3% of the Alz50-positive neurons in EC expressed human tau mRNA at 12 months, indicating a spread of misfolded tau to neighboring neurons within the EC without detectable transgene expression (Figure 3F). By 24 months of age, an astonishing 97% of Alz50-positive neurons (96.4% ± 6.45% SD; $p < 0.001$) did not have any detectable human transgene expression, showing that the propagation to neighboring cells increased with age (Figure 3F) and indicating that transgene expressing neurons may be lost (as will be discussed later).

Alz50-positive aggregates were also found in large numbers of neurons without detectable transgene expression in the DG, anterior cingulate cortex, CA1, and CA3, all major targets of the EC (Witter et al., 1988). Importantly, unlike the anterior cingulate cortex, cortical areas that showed limited transgene expression outside of the EC, but do not receive direct input from the EC, did not show any tau aggregation. Moreover, the cerebellum, which expresses human P301L tau mRNA, did not develop any fibrillar accumulation of htau in the soma.

These experiments with FISH showing human tau protein and Alz50-positive aggregates in cells without detectable levels of human tau mRNA confirm the transmission of human tau from neuron to neuron and rule out the possibility that the transgene promoter was nonspecifically expressing human tau in these hippocampal neurons (i.e., becoming "leaky" in older animals).

To confirm that the absence of human tau mRNA in the FISH experiments was not due to limited sensitivity of the technique,

we used FISH to label human tau mRNA and immunofluorescence with HT7 to label human tau protein in sections from 17-month-old animals. We then used laser capture microscopy to capture three different populations of cells on an individual cell-by-cell basis for analysis by qPCR: (1) neurons negative for human tau mRNA and negative for human tau protein; (2) neurons negative for human tau mRNA and positive for human tau protein; (3) neurons positive for human tau mRNA and positive for human tau protein (Figure 3E). Total RNA was extracted and qPCR analysis of the complementary DNA (cDNA) product was carried out using primers against the transgenic human tau construct. The qPCR data clearly show that the neurons that were human tau protein-positive and RNA-negative by FISH indeed did not express detectable levels of the tau transgene (Figure 3G), in contrast to robust detection of tau mRNA in neurons positive for tau mRNA by FISH. Taken together, these data strongly suggest that the human tau protein may be undergoing neuron-to-neuron transmission.

Human Tau Seeds Mouse Tau Aggregation

The above experiments strongly suggest the spread of human tau protein from neuron to neuron, which could cause seeding of misfolding and aggregation of tau. It has been shown in cell culture experiments that extracellular tau aggregates could be internalized transmitting tau misfolding from the outside to the inside of the cell, where these aggregates could seed fibril formation of recombinant tau monomer. Moreover, the same study showed that tau aggregates were transferred between cocultured cells (Frost et al., 2009). Another recent study reported that brain extracts from neurofibrillary tangle-bearing mouse brain injected in wild-type tau-expressing mice induces seeding of tau fibrils in neurons (Clavaguera et al., 2009).

To determine whether mouse tau is recruited by human tau to aggregate, we performed immunohistochemical analysis using an antibody specific for mouse tau that revealed that mouse tau indeed accumulates in the somatodendritic compartment of MEC neurons of 24-month-old rTgTauEC mice (Figure 4A). Age-matched control mice have diffuse axonal staining with the mouse tau antibody, and tau knockout mice show no immunoreactivity, as expected. Human AD cases also have no immunoreactivity to mouse tau, indicating that the observed immunoreactivity is not due to human tau becoming reactive to the mouse tau antibody during pathological changes. Results from double labeling using Alz50 and mouse tau antibodies showed that Alz50 and mouse tau staining colocalized in neuronal cell bodies of the MEC, which is further evidence for mouse tau recruitment into aggregates in the rTgTauEC mouse model (Figure 4B). Immunoblotting using the mouse tau-specific antibody also revealed that mouse tau increased with age in rTgTauEC mice (Figure 4C), indicating that it may accumulate in tangles. In confirmation of this idea, sarkosyl-insoluble and -soluble fractions both contain endogenous mouse tau (Figure 4D). The specificity of the mouse tau antibody was confirmed by western blot analysis (Figure 4E), which revealed mouse tau (mTau) reactivity in rTgTauEC and control mouse brain but not in tau knockout mouse brain or human AD brain.

These data suggest that human tau enters neighboring cells that do not have detectable levels of human tau transgene and transmits a misfolded state that recruits endogenous mouse tau into the somatodendritic compartment, where it becomes misfolded and contributes to tau aggregation.

Progressive Neurodegeneration and Gliosis in rTgTauEC Neural Circuits

Tau pathology in rTgTauEC mice was first observed as Alz50 staining in the axon terminals from the perforant pathway arising in EC-II terminating in the middle molecular layer of the DG (Table S1). This has also been observed in AD patients (Hyman et al., 1988) and suggests that conformationally abnormal tau is axonally transported along the perforant pathway to presynaptic axon terminals, or that the Alz50 epitope is generated first at the axon terminals. We observed age-dependent degeneration of axon terminals in rTgTauEC mice (Figure 5A; for higher magnification images, see Figure S2; for pathology progression, see Table S1). Alz50 tau staining of misfolded tau in axon terminals increased with age through 12 months (Figure 5A, second left panel). At 18 months, the reactivity in axon terminals decreased and staining in soma of the molecular layer of the DG became more prominent, indicating the possibility that EC-II axons began to degenerate and DG granular neurons took up the misfolded protein (Figure 5A, middle panel). From 21 months of age, the pattern of Alz50 reactivity in the middle molecular layer of the DG changed from a clear layer to irregular patches in the axon terminal zone (Figure 5A, right panels), similar to a pattern observed in AD patients (Hyman et al., 1988).

Axonal degeneration was accompanied by gliosis in rTgTauEC brain. rTgTauEC mice showed evidence of microglial activation (Figures 5B and 5C) and astrogliosis (Figures 5D and 5E). At 24 months of age, Alz50-positive patches of axon terminals in the middle molecular layer were surrounded by activated microglia (Figure 5C), suggesting that axon terminals and their synapses were degenerating in this area. Double labeling using PHF1, phosphorylated tau antibody, and glial fibrillary acidic protein (GFAP) antibody demonstrated reactive astrocytes that were PHF1-positive at 24 months of age (Figure 5E). The tau transgene is not expressed in glia, and there were no PHF1-positive astrocytes at earlier ages, indicating that human tau is likely released from terminals and taken up by glia as the axons degenerate.

The irregular patches of Alz50 staining of EC-II axon terminals surrounded by activated microglia suggest that synapses are lost in this region as axons degenerate. Previous studies have shown that partial deafferentation of granule cells of the dentate gyrus during normal aging was caused by a loss of axodendritic synapses in the molecular layer, and a loss of axosomatic synapses (Geinisman, 1979; Geinisman et al., 1977). In AD, early hallmarks include the loss of synapses, and comparison of AD patients to age-matched control individuals showed that the density of synapses correlated strongly with cognitive impairment, suggesting that loss of connections is associated with the progression of the disease (DeKosky and Scheff, 1990; Scheff and Price, 2006; Terry et al., 1991). Therefore, we assessed two synaptic markers in the perforant pathway terminal zone of rTgTauEC mice: synapsin-I, a marker of synaptic vesicles, and PSD-95, a postsynaptic marker that has been reported to decrease early in neurodegeneration (Zhao et al., 2006)

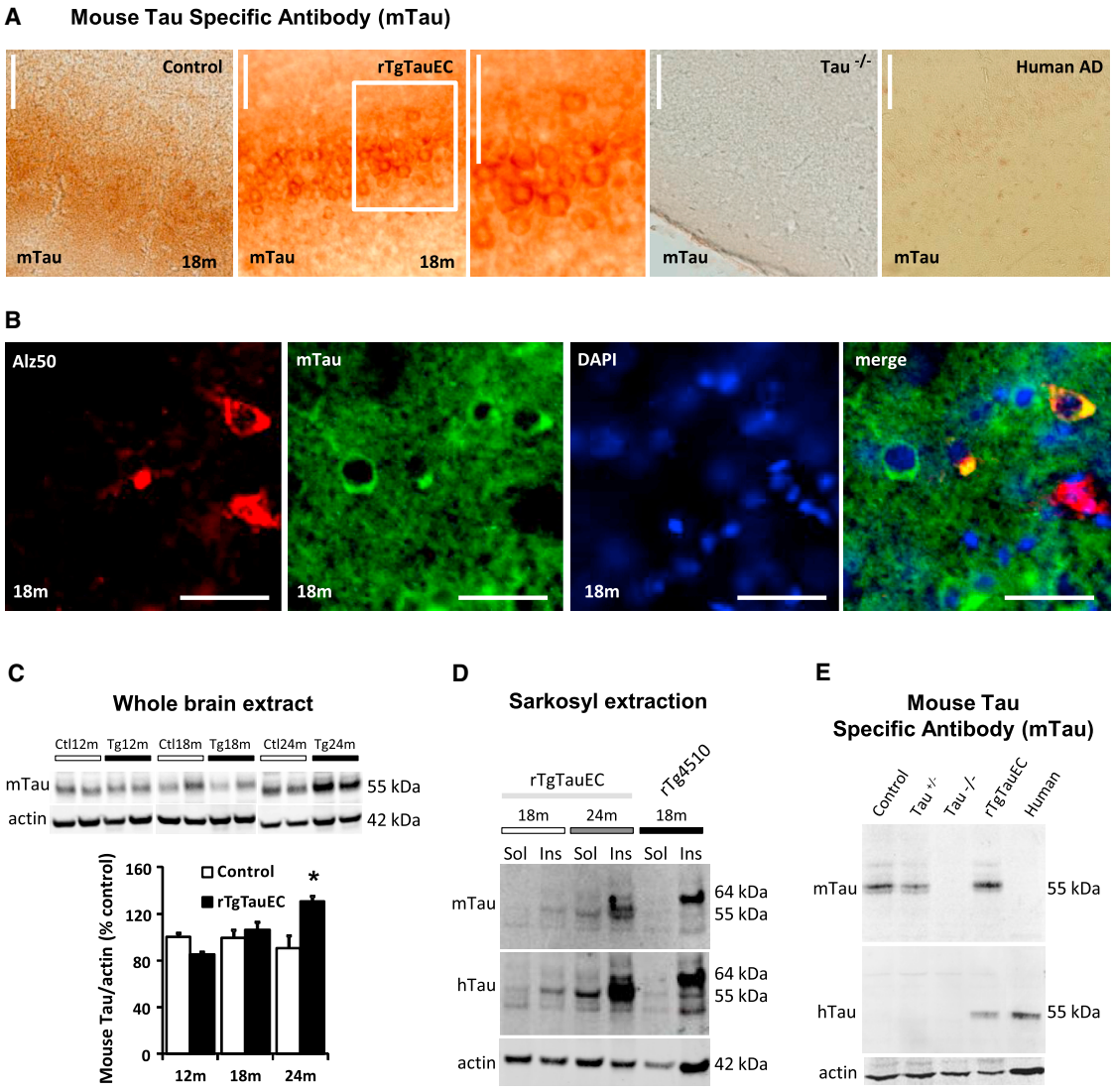

Figure 4. Human Tau Protein Seeds Endogenous Mouse Tau Pathology

(A) Immunohistochemistry using a mouse-specific tau antibody (mTau) shows normal axonal distribution of mouse tau in control mice and somatodendritic accumulation of mouse tau in rTgTauEC mice in the EC at 18 months of age. The mTau antibody showed no staining in tau knockout mice or human AD brain. Scale bars, 100 μm.

(B) Double labeling using Alz50 and mouse tau antibodies shows that Alz50 and mouse tau staining colocalize in neuronal cell bodies. Scale bar, 20 μm.

(C) Whole brain extracts from rTgTauEC mice at different ages show an age-dependent increase in mouse tau. Representative blots are shown at the top, and quantification is shown at the bottom (n = 4 mice per group). Results are expressed as the mean ± SEM. *$p < 0.05$.

(D) Sarkosyl-insoluble and -soluble fractions from whole brain of 18- and 24-month-old rTgTauEC probed using mTau revealed that sarkosyl-insoluble and -soluble fractions both contain endogenous mouse tau.

(E) Immunoblotting of brain extracts using mTau confirmed its specificity, since it does not recognize protein in tau knockout brain or human AD brain.

(Figure 6A). We used array tomography to allow high-resolution, quantitative measurement of synaptic densities. We found that both pre- and postsynaptic densities were significantly reduced in the middle third of the molecular layer at 24 months of age in tau-expressing transgenic mice (Figure 6B).

To estimate neuronal loss, neuronal counts in the EC and hippocampal subareas were performed on transgenic and control animals at 21 and 24 months of age (n = 3 to 4 animals per group), using stereological estimations of cresyl violet-labeled neuronal nuclei. Neurons were identified by their morphology. In rTgTauEC mice, significant neuronal loss was detected at 24 months of age in the areas of transgene expression, EC-II, and parasubiculum, compared to the average neuron number in age-matched control brains (Figure 6C). We observed a 42% decrease in neuron density in EC-II. We did not observe significant neuronal loss up to 21 months of age. Quantification by stereological counts showed that 47% of all neurons in the EC-II were Alz50-positive at 12 months of age; this figure

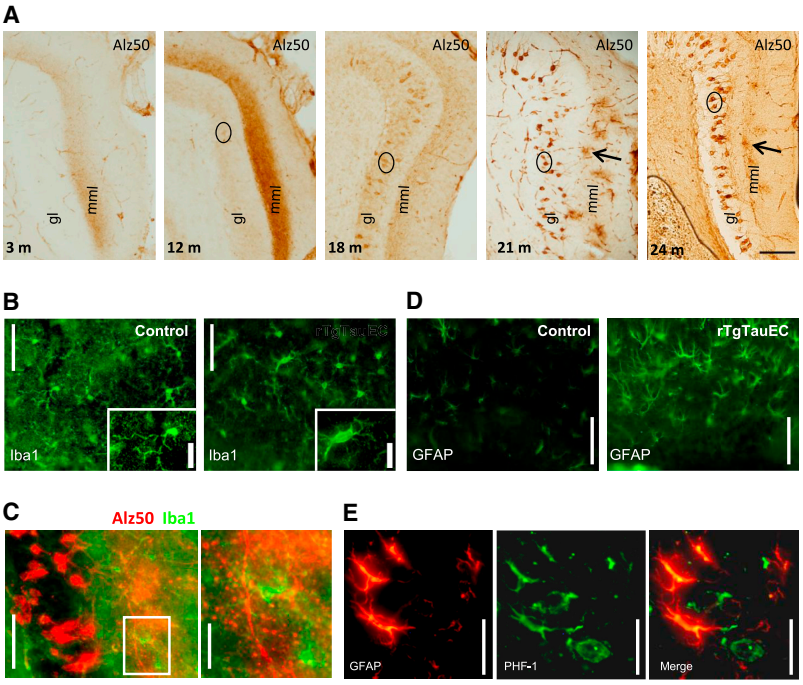

Figure 5. Axon Terminals Degenerate Progressively in the Terminal Zone of EC-II Axons

(A) The terminal zone of axonal projections from the layer II MEC neurons with the granular layer (gl) and the middle molecular layers (mml) that express the human tau transgene developed early accumulation of misfolded tau (Alz50 staining, which intensified up to 12 months of age. At 18 months, the terminal staining with Alz50 became fainter with DG neurons in the granular cell layer becoming more prominently stained. At 21 and 24 months, Alz50 staining in the terminal zone was patchy, indicating degeneration of Alz50-containing axons (scale bar, 100 μm).

(B) Concomitant with this axonal degeneration, we observed increased microglial activation (Iba1 staining) at 24 months of age in rTgTauEC mice in the molecular layer of the DG. Scale bars, 50 μm (left panel), 20 μm (right panel).

(C) Double immuno-histolabeling with Alz50 and Iba1 shows that the patches of Alz50 staining of the axon terminals in the middle molecular layer of the DG are surrounded by activated microglia (shown in higher magnification in the inset). Scale bars, 50 μm (left panel), 20 μm (right panel).

(D) GFAP-labeled astrocytes are more prevalent in rTgTauEC brain than controls. Scale bars, 50 μm.

(E) Colocalization of GFAP- and PHF1-positive aggregates indicate uptake of tau by astrocytes. Scale bars, 20 μm.

dropped to approximately 10% at 24 months of age (Figure 6D), as some neurons died.

We hypothesize that the observed age-associated neurodegeneration is due to the age-dependent toxicity of tau that is pathologically mislocalized to the soma, hyperphosphorylated, and aggregated, similar to observations in human AD brain. To formally exclude the possibility that axonal degeneration and neuronal loss at 24 months are not due to increased transgene expression at later ages, we quantified the percentage of neurons expressing the human tau transgene. Stereological counts of human tau-expressing neurons labeled with FISH show that approximately 12% of neurons (12.4% ± 1.69% SEM) in EC-II expressed the transgene at 3 months of age (Figures 6E and 6F). This number was unchanged at 12 months (13.21% ± 0.86% SEM; $p = 0.366$) and 18 months of age (12.18% ± 1.96 SEM; $p = 0.481$), showing that only a portion of neurons in the EC-II expressed the human tau transgene. At 24 months of age, only ~4% (3.71% ± 0.84% SEM) of the neurons expressed the transgene (Figures 1C and 1D) ($p < 0.005$). The pattern of human tau protein expression also changes as the animals age. There is a significant reduction in the human tau immunofluorescence staining of the EC at 24 months, and the cell bodies of the DG neurons become immunoreactive for human tau, suggesting that the protein is being transmitted (Figure S4).

Together, these data indicate that neurodegeneration begins in this model of early AD with degeneration of axon terminals followed by loss of synapses and neurons. Further, the cell loss observed at 24 months exceeds the number of neurons that were expressing the transgene, suggesting that neurons that develop tau pathology without expressing the transgene might also be lost.

DISCUSSION

To understand the sequence of events from expression of pathological tau in the EC to the development of widespread cortical involvement, we recreated an early stage of AD neurofibrillary pathology in transgenic mice to investigate how, starting in the entorhinal area, tau pathology leads to neural system dysfunction. We observed two important consequences of the formation of tangles in the EC: (1) spreading of the pathology to downstream connected neurons despite regional and cellular restriction of transgene expression, and (2) evidence favoring very slow synaptic, then axonal, then somatic degeneration associated with accumulation of misfolded tau.

Recent data suggest that intracellular protein aggregates of tau have the capacity to seed aggregation of native tau proteins and might propagate their misfolded state in a prion-like manner. This transmission has first been described to occur inside cells, since incorrectly folded tau proteins convert to an aggregate-prone state acting as a nucleus that recruits additional tau monomers (de Calignon et al., 2010; Iliev et al., 2006; Mocanu et al., 2008). In cell culture experiments (Frost et al., 2009), extracellular tau aggregates could enter cells and trigger tau fibrillization. In living mouse brain, intracortical injections of tau aggregates seed tau fibrillization in neurons carrying the human transgene (Clavaguera et al., 2009). Here, we found that in aged rTgTauEC mice, human tau protein is present in neurons that do not have detectable levels of human tau mRNA, suggesting that transneuronal propagation of tau occurs. This idea is also supported by our data showing that (1) in EC-II, the number of transgene-expressing neurons decreases in older age, correlating with neuronal loss, while (2) the proportion of transgene-negative Alz50-positive neurons robustly increases with age, suggesting

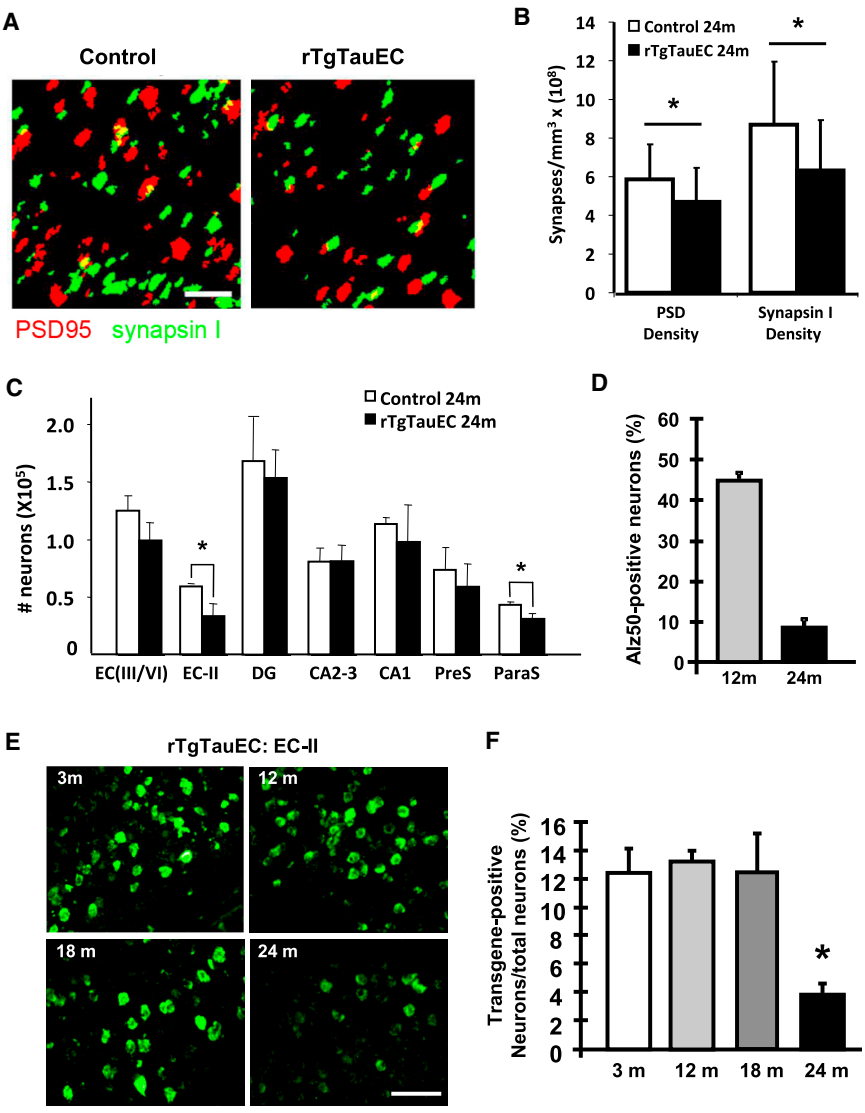

Figure 6. Synaptic Loss in the Target Zone of the Perforant Pathway and Loss of EC-II Neurons in rTgTauEC Mice

(A and B) Array tomography using synapsin I (green) and PSD95 (red) to label pre- and postsynaptic structures in the middle molecular layer of the DG (scale bar, 2 μm) shows pre- and postsynaptic loss at 24 months of age in the middle molecular layer of the DG, indicating loss of synapses between EC-II neurons and DG neurons.

(C) Numbers of neurons were estimated by stereology for different areas of the brain (PreS, presubiculum; ParaS, parasubiculum). Significant neuronal loss was detected at 24 months of age in EC-II and the parasubiculum compared to age-matched control brain.

(D) Similar stereological quantification showed that 47% of neurons in the EC were Alz50-positive at 12 months of age and ~10% were Alz50-positive at 24 months of age.

(E and F) Levels of transgene expression. Loss of neurons could not be explained by an increase in transgene expression with age, since the level of transgene expression assessed by stereological counts of tau mRNA-positive neurons labeled with FISH showed that the level of transgene expression in MEC did not change from 3 to 18 months of age and significantly decreased at 24 months (scale bar, 100 μm). Results are expressed as the mean ± SEM. *$p < 0.05$.

that the remaining Alz50-positive neurons were secondarily affected by transneuronal transfer. It has been reported that glial tau pathology occurs in tauopathies (Ballatore et al., 2007; Chin and Goldman, 1996) and in AD (Nakano et al., 1992; Nishimura et al., 1995; Papasozomenos, 1989a, 1989b), where tau inclusions can be found in astrocytes and oligodendrocytes. The presence of human tau protein in GFAP-positive astrocytes in rTgTauEC mice suggests that release of tau from neurons and uptake by glia also takes place in this model.

The specificity of the neuropsin-driven transactivator for EC and related structures was demonstrated by FISH, qPCR, immunostaining, and western blot analysis of rTgTauEC mice. Moreover, the parental P301L mice without the transactivator transgene showed levels of human tau protein or mRNA (Figure S1) below detection thresholds, in accord with a recent observation that the "tau alone" parental line expresses <2% of the levels of rTg4510 mice and does not develop any tau pathological alterations with age (Barten et al., 2011).

Taken together, the data presented in this study indicate that, in rTgTauEC mice, tau was not only transferred to neighboring cells, but also to synaptically connected neurons, which suggests that tau—or a particular species of tau, such as hyperphosphorylated tau, misfolded tau, or a fragment of tau—may have been released at the synapse. In the DG, CA regions, and cingulate cortex, we found neurons that do not have detectable human tau mRNA at any of the ages examined, which accumulated tau immunoreactive species (recognized by multiple antibodies) at advanced ages (21 and 24 months). In parallel to our study, a recent report described a mouse model of mutant amyloid precursor protein expressed predominantly in the EC that used the same promoter as that of rTgTauEC mice. Progression of Aβ deposition to the hippocampus and cingulate cortex was also reported (Harris et al., 2010). These data suggest that misfolded tau and Aβ share properties that allow propagation through the extracellular space to disrupt neuronal systems.

Our data support the idea that tau, when accumulated in the terminal zones, induces synaptic destruction. We cannot distinguish between the possibilities that misfolded axonal tau induces dying back terminal degeneration, or that release of tau is synaptotoxic. It is not clear how, or if, misfolded tau gets released and/or taken up by neurons, but the presence of increased tau cerebrospinal fluid levels after injury is consistent

with the possibility that injury induces release (Blennow et al., 1995). In rTgTauEC mice, propagation seems more tightly linked to the time frame when axons are dying back (21–24 months) than when Alz50-positive tau can be detected in axon terminals (3 months), but this does not preclude the possibility that some tau is released and taken up at earlier ages, even under normal physiological circumstances.

Interestingly, by using a specific mouse tau antibody, we also show evidence that endogenous mouse tau accumulates in the somatodendritic compartment of EC neurons, where it coaggregates with human tau. Furthermore, we also report that mouse tau can be detected in both the sarkosyl-soluble and -insoluble fractions, suggesting that misfolded human tau can recruit endogenous mouse tau to aggregate.

If the propagation of AD tangle pathology from Braak stage I to VI entails, to some extent, the type of neuronal system propagation events described here, several critical questions remain. (1) Why are some neuronal populations protected from developing tangles despite being anatomically strongly connected to neuronal populations that do develop tangles? (2) Does tau need to emerge into the extracellular space where it is potentially available to therapies such as immunotherapy, or might it be released from the cytoplasm, yet remain sequestered within membrane-bound compartments such as exosomes? (3) Which species of tau are responsible for transferring the aggregated state to nonexpressing cells? (4) Is the tau that is capable of initiating misfolded aggregates in downstream cells an aggregated form or a consequence of a unique posttranslational modification such as phosphorylation, acetylation, glycosylation, or truncation? Understanding these issues may help inform therapeutic approaches that have promise to slow the progression of AD.

EXPERIMENTAL PROCEDURES

Animals

We generated the line of transgenic animals (called rTgTauEC [reversible tau restricted to EC]) by crossing FVB-Tg(tetO-Tau$_{P301L}$)4510 mice (Santacruz et al., 2005) with a transgenic mouse line on a C57BL/6 genetic background expressing tet transactivator under the control of the neuropsin promoter (developed at The Scripps Research Institute [Yasuda and Mayford, 2006]). Only F1 offspring were used as experimental animals, ensuring a uniform 50:50 mix of FVB and C57BL/6 genetic background. The human Tau gene with the P301L mutation in rTg4510 mice is downstream of a tetracycline-operon responsive element and requires the presence of the tet transactivator (Gossen and Bujard, 1992). Since the tet transactivator is downstream of the promoter of neuropsin, human tau$_{P301L}$ expression is restricted to EC-II. Mice with both the activator and responder transgenes are abbreviated rTgTauEC. Age-matched littermates expressing only the activator transgene and the responder transgene were used as controls. Mice were screened by PCR using the primer pairs 5′-ACCTGGACATGCTGTGATAA-3′and 5′-TGCTCCCATT CATCAGTTCC-3′ for activator transgenes and 5′-TGA ACC AGG ATG GCT GAG CC-3′ and 5′-TTG TCA TCG CTT CCA GTC CCC G-3′ for responder transgenes. Each of the eight age groups studied (3, 6, 9, 12, 15, 18, 21, 24 months) contained transgenic and control animals. A total of 183 animals were used for this study, including 97 transgenic and 86 control animals.

All animal experiments were performed in accordance with national guidelines (National Institutes of Health) and approved by Massachusetts General Hospital and McLaughlin Institute Institutional Animal Care and Use Committees.

Human Subject

Formalin-fixed, paraffin-embedded tissue specimens and frozen tissue from the temporal association isocortex (Brodmann area 38) of one patient with AD was obtained from the Massachusetts Alzheimer Disease Research Center Brain Bank. The study subject and their next of kin gave written informed consent for the brain donation, and the Massachusetts General Hospital Institutional Review Board approved the study protocol. The subject fulfilled the National Institute of Neurological and Communicative Disorders Alzheimer's Disease and Related Disorders Association criteria for probable AD and the National Institute on Aging-Reagan criteria for high likelihood of AD.

Stereology and Immunocytochemistry

The animals were euthanized by CO_2 asphyxiation and the brains harvested, fixed in 4% paraformaldehyde containing 15% glycerol cryoprotectant for 2 to 3 days, then either sectioned or stored at 4°C in a 20% sucrose solution. The brains were frozen and serial horizontal sections 40 μm thick were cut on a freezing sliding microtome. Groups of every 10 sections were used to characterize each brain.

An unbiased stereologic counting method was used to determine the number of neurons per region of the brain (Hyman et al., 1998). The optical dissector technique was used in a similar fashion to previously described work in transgenic mice (Irizarry et al., 1997). The image analysis system NewCAST (stereology module for VIS; Visiopharm Integration System ver. 2.12.3.0, Denmark), mounted on an upright Olympus BX51 microscope (Olympus, Denmark) with an integrated motorized stage (PRIOR-Proscan II, Prior Scientific, Rockland, MA) was used to outline regions, sample, and count.

Counting frames of size 21.8 μm × 21.8 μm, and step length from 100 μm to 200 μm were selected to count >200 neurons per animal. The different brain regions were defined using the atlas developed by Franklin and Paxinos (2007). The differentiation between the MEC and LEC was made using the atlas mentioned above and the mapping of van Groen (2001).

Standard immunofluorescence techniques were used to label Tau epitopes.

Endogenous peroxidase activity was quenched for 30 min in H_2O_2. After blocking in 5% milk for 1 hr, the appropriate primary antibody was applied, and sections were incubated overnight at 4°C. Sections were subsequently washed in Tris-buffered saline (TBS) to remove excess primary antibody. Sections were incubated in the appropriate secondary antibody for 1 hr at room temperature. After serial washes in TBS, slides were developed with diaminobenzidine substrate by using the avidin-biotin horseradish peroxidase system (Vector Laboratories). Fluorescent CY3-labeled secondary antibody (Invitrogen) was used to reveal 5A6.

The antibodies with 5A6 (generated by G.V. Johnson, 1997; 1:1,000), HT7 (Thermo Scientific; 1:1,000), and TauY9 (Enzo Life Sciences; 1:1,000) were used to specifically detect human tau; the conformation-specific Alz50 antibody (courtesy of Peter Davies, Albert Einstein College of Medicine; 1:50) and phosphorylated 396/404 tau PHF1 (courtesy of Peter Davies; 1:500) antibodies were used to detect pretangle stages. Fluorescent CY3-labeled secondary antibody (Invitrogen) was used to reveal HT7, and nonfluorescent biotinylated secondary antibodies revealed by diaminobenzidine were used to detect Alz50 and PHF1. The antibody Iba1 (Wako, 1:1,000) was used to reveal microglia. Activated astrocytes were labeled using the GFAP antibody (Sigma, 1:1,000).

mTau is a polyclonal rabbit antibody that was generated by Dr. Naruhiko Sahara. Briefly, mTau was raised against a mouse tau epitope, which is absent in the human tau sequence and corresponds to amino acid residues 118–131 (SKDRTGNDEKKAKG). The antibody was characterized by western blot analysis and immunohistochemistry for sensitivity and specificity and did not recognize any unspecific proteins in tau knockout (KO) mice or in human brain. Tau KO mice, which have a targeted disruption of exon 1 of tau (Tucker et al., 2001), were used for the characterization of the mTau antibody. Tau KO mice were bred with C57Bl/6 mice to produce tau KO heterozygote mice also used in the antibody characterization.

Gallyas silver staining was performed on brain sections according to previous description (Gallyas, 1971). Thioflavin S staining was performed by leaving the mounted sections for 8 min in a solution of 0.05% Thioflavin S in 50% ethanol (EtOH), rinsed in ethanol 100%, then water (Sun et al., 2002).

Images for figures were collected on an upright Olympus BX51 microscope (Olympus America, Center Valley, PA).

In Situ Hybridization and Riboprobe Generation

Colorimetric in situ hybridization and riboprobe generation were performed as previously described (Schaeren-Wiemers and Gerfin-Moser, 1993). FISH with

Alz50 co-immunohistochemistry was performed as previously described (Price et al., 2002). Riboprobe templates were generated by RT-PCR from mouse and human brain tissue and correspond to the 3′ untranslated regions of mouse Mapt (NM_001038609.1; nucleotides 1606–2588) and human Mapt (NM_016835; nucleotides 2773–3602).

Laser Capture Microdissection and qPCR Analysis following FISH and Immunofluorescence

Cryosections (10 μm) of snap-frozen brains from 24-month-old rTgTauEC mice were collected on microscopy slides (Gold Seal Rite-On Micro Slides, Portsmouth, NH). Following FISH, each tissue section was fixed in 70% EtOH for 40 s, rinsed with RNase-free PBS, incubated with the human tau-specific HT7 antibody in PBS for 10 min, rinsed with PBS, incubated with Alexa 488 goat anti-mouse immunoglobulin G (IgG) (Invitrogen) in PBS for 10 min, rinsed with PBS followed by dehydration in increasingly concentrated EtOH 70%–100% into xylene. Different populations of cells were captured after FISH and immunofluorescence that can be divided into three groups: (1) tau mRNA-negative and human protein negative neurons; (2) mRNA-negative and human tau protein-positive neurons; and (3) transgene mRNA-positive and human tau protein-positive neurons. Approximately 500 cells from EC-II and the DG were captured per group onto separate polyethylene collecting caps (Macro Cap, Arcturus, MDS Analytical Technologies, Sunnyvale, CA). Total RNA was extracted using the Arcturus PicoPure RNA isolation kit per the manufacturer's instructions. Samples were eluted in 14 μl. RNA samples were assayed for quality with an Agilent 6000 Bioanalyzer and a Nanodrop spectrophotometer. Reverse transcription was carried out on all RNA samples (Superscript II, Invitrogen) and random hexamers. qPCR analysis (on Bio-Rad iCycler) of the cDNA product was carried out using primers against the transgenic human tau construct (5′-CCC AAT CAC TGC CTA TAC CC-3′ and 5′-CCA CGA GAA TGC GAA GGA-3′), mouse tau exon 7 (5′-AGC CCT AAG ACT CCT CCA-3′ and 5′-TGC TGT AGC CGC TTC GTT CT-3′), and glyceraldehyde-3-phosphate dehydrogenase (5′-TGG TGA AGC AGG CAT CTG AG-3′ and 5′-TGC TGT TGA AGT CGC AGG AG-3′). Triplicates of cDNA samples were added to a 25 μl reaction containing 12.5 μl SYBR green Mastermix (Applied Biotechnology). For the standard curve, we subcloned cDNA amplicons generated using the qPCR primers in the pcDNA 3.1 vector system (Invitrogen) according to the manufacturer's instructions. After verifying the respective specificities of the cDNA clones by sequencing, these were used to generate individual standard curves, thus allowing for calculation of molarity and number of mRNA molecules in the samples. Finally, the respective tau mRNA levels were normalized to murine tau mRNA levels.

Western Blot Analysis

Animals were sacrificed by decapitation, the brains were extracted, and either the brain or hippocampi and EC were dissected. Tissue was homogenized in radio-immunoprecipitation assay buffer (Sigma) supplemented with a cocktail of protease and phosphatase inhibitors (Roche). Samples were homogenized using a Polytron and stored at −80°C. The materials for SDS-PAGE were obtained from Invitrogen (NuPAGE system). Protein lysates were boiled in sample buffer consisting of lithium dodecyl sulfate sample buffer and reducing agent and resolved on 4%–12% Bis-Tris polyacrylamide precast gels in a 3-(n-morpholino)propanesulfonic acid-SDS running buffer containing antioxidant. For most analyses, 30 μg/lane were loaded, unless indicated otherwise. Gels were transferred onto Nitrocellulose Membranes Protran (Whatman) in transfer buffer containing 20% methanol. Blots were blocked in Odyssey blocking buffer (Li-Cor biosciences), followed by incubation with primary antibodies (β -actin [Sigma; 1:10,000]; Total Tau [Dako; 1:10,000], HT7 [1:5,000], TauY9 [1;1,1000], mTau [Naruhiko Sahara; 1:5,000], AT180 [pT231, Thermo Scientific; 1:1,000], PHF1 [courtesy of Peter Davies; 1:5,000], CP13 [courtesy of Peter Davies, 1:1,000], and DA9 [courtesy of Peter Davies; 1: 10,000]) and detected with anti-mouse or anti-rabbit IgG conjugated to IRDye 680 or 800 (Li-Cor Biosciences; 1:10,000). Densitometric and MW analyses were performed using ImageJ software (National Institutes of Health). Band density values were normalized to β-actin or total tau levels when tau phosphorylation levels were analyzed. Mean band densities for samples from rTgTauEC mice were normalized to corresponding samples from control mice.

Sarkosyl Insolubility Assay

Purification of sarkosyl-insoluble tau was performed as previously described (Hasegawa et al., 2007) with slight modifications. Briefly, whole frozen brains of 24- and 18-month-old rTgTauEC (n = 3), control (n = 3), and 18-month-old rTg4510 (n = 1) mice were homogenized by polytron in 10 volumes of buffer H (10 mM Tris-HCl [pH 7.5] containing 0.8M NaCl, 1 mM EGTA, and 1 mM dithiothreitol) and spun at 100,000 × *g* for 30 min at 4°C. Another 2 ml of buffer H was added to the pellet and the samples were homogenized again by polytron, incubated in 1% Triton X-100 at 37°C for 30 min. Following the incubation, the samples were spun at 100,000 × *g* for 30 min at 4°C, the pellet was homogenized by polytron on 1 ml of buffer H and was then incubated in 1% sarkosyl at 37°C for 30 min and spun at 100,000 × *g* for 30 min at 4°C. The supernatant was then collected (sarkosyl-soluble fraction). Detergent-insoluble pellets were extracted in 100 μl of urea buffer (8 M urea, 50 mM Tris-HCl [pH 7.5]), sonicated, and spun at 100,000 × *g* for 30 min at 4°C. The supernatant was then collected (sarkosyl-insoluble fraction). The protein concentration of extracts was determined by BCA assay (Thermo Scientific), and either 25 μg/lane (rTgTauEC) or 5 μg/lane (rTg4510) were loaded were loaded. Sarkosyl-insoluble and -soluble fractions were run on SDS-PAGE gels (4%–20%), transferred to nitrocellulose membranes, and probed with total tau DA9 (epitope: aa 112–129) mouse monoclonal antibody (courtesy of Peter Davies; 1:1,000). The DA9 antibody recognizes both human and mouse tau proteins and was generated against human tau preparations (Tremblay et al., 2010).

Array Tomography

Tissue blocks from the DG of 21- and 24-month-old rTgTauEC (n = 3 at 21 months, n = 3 at 24 months) mice and littermate controls (n = 5 at 21 months, n = 3 at 24 months) were prepared for array tomography as described previously (Koffie et al., 2009; Micheva and Smith, 2007). Briefly, mice were sacrificed using carbon dioxide, brains were removed, and small blocks containing DG were dissected, fixed in 4% paraformaldehyde with 2.5% sucrose in PBS for 2 hr, dehydrated, and embedded in LR White resin (Electron Microscopy Sciences, Hatfield, PA). Ribbons of ultrathin sections (70 nm) were collected on slides and stained with antibodies to synapsin I (rabbit polyclonal Ab1543 Millipore, Billerica, MA), PSD95 (goat polyclonal Abcam Ab12093, Cambridge, MA), and secondary donkey anti-rabbit Cy3 and donkey anti-goat Cy5 (Jackson ImmunoResearch, West Grove, PA) counterstained with a fluorescent Nissl counterstain (NeuroTrace blue, N21479, Invitrogen, Carlsbad, CA). Images of the same area of the middle molecular layer of the DG were obtained on 7–11 serial sections in two different sample sites per animal using a Leica TCS SL confocal system (Leica Microsystems Bannockburn, IL). Images were made into stacks and aligned using ImageJ software. Three to six crop boxes were chosen in each stack in a region free of nuclei. Each crop was analyzed using the watershed program (generously provided by B. Busse and Stephen Smith) to count puncta that are present in more than one consecutive image in the stack to remove noise.

Data were analyzed using JMP (SAS Institute, Cary, NC). Normality of the data was tested using a Shapiro-Wilks test. One-way analysis of variance was used to compare means of the different genotypes. Data are presented as the mean ± SEM.

SUPPLEMENTAL INFORMATION

Supplemental Information includes four figures and one table and can be found with this article online at doi:10.1016/j.neuron.2011.11.033.

ACKNOWLEDGMENTS

This work was supported by an Alzheimer's Association Zenith award; National Institutes of Health grants AG08487, AG026249, K08NS069811, K99AG33670, R21AG038835-01A1, and R21 NS067127; and American Health Assistance Foundation grant A2011086. We thank Mark Mayford for providing neuropsin-tTA mice, Peter Davies for providing tau antibodies, and Zhanyun Fan, Taylor Friedman, Charles Vanderburg, Ozge Cagsal-Getkin, and Meredith Banigan for technical assistance.

Accepted: November 30, 2011
Published: February 22, 2012

REFERENCES

Ballatore, C., Lee, V.M., and Trojanowski, J.Q. (2007). Tau-mediated neurodegeneration in Alzheimer's disease and related disorders. Nat. Rev. Neurosci. *8*, 663–672.

Barten, D.M., Cadelina, G.W., Hoque, N., DeCarr, L.B., Guss, V.L., Yang, L., Sankaranarayanan, S., Wes, P.D., Flynn, M.E., Meredith, J.E., et al. (2011). Tau transgenic mice as models for cerebrospinal fluid tau biomarkers. J. Alzheimers Dis. *24* (*Suppl 2*), 127–141.

Blennow, K., Wallin, A., Agren, H., Spenger, C., Siegfried, J., and Vanmechelen, E. (1995). Tau protein in cerebrospinal fluid: a biochemical marker for axonal degeneration in Alzheimer disease? Mol. Chem. Neuropathol. *26*, 231–245.

Braak, H., and Braak, E. (1991). Neuropathological stageing of Alzheimer-related changes. Acta Neuropathol. *82*, 239–259.

Canto, C.B., Wouterlood, F.G., and Witter, M.P. (2008). What does the anatomical organization of the entorhinal cortex tell us? Neural Plast. *2008*, 381243.

Chin, S.S., and Goldman, J.E. (1996). Glial inclusions in CNS degenerative diseases. J. Neuropathol. Exp. Neurol. *55*, 499–508.

Clavaguera, F., Bolmont, T., Crowther, R.A., Abramowski, D., Frank, S., Probst, A., Fraser, G., Stalder, A.K., Beibel, M., Staufenbiel, M., et al. (2009). Transmission and spreading of tauopathy in transgenic mouse brain. Nat. Cell Biol. *11*, 909–913.

de Calignon, A., Fox, L.M., Pitstick, R., Carlson, G.A., Bacskai, B.J., Spires-Jones, T.L., and Hyman, B.T. (2010). Caspase activation precedes and leads to tangles. Nature *464*, 1201–1204.

DeKosky, S.T., and Scheff, S.W. (1990). Synapse loss in frontal cortex biopsies in Alzheimer's disease: correlation with cognitive severity. Ann. Neurol. *27*, 457–464.

Delacourte, A., David, J.P., Sergeant, N., Buée, L., Wattez, A., Vermersch, P., Ghozali, F., Fallet-Bianco, C., Pasquier, F., Lebert, F., et al. (1999). The biochemical pathway of neurofibrillary degeneration in aging and Alzheimer's disease. Neurology *52*, 1158–1165.

Franklin, K., and Paxinos, G. (2007). The Mouse Brain in Stereotaxic Coordinates, Third Edition (San Diego, CA: Academic Press).

Frost, B., Jacks, R.L., and Diamond, M.I. (2009). Propagation of tau misfolding from the outside to the inside of a cell. J. Biol. Chem. *284*, 12845–12852.

Gallyas, F. (1971). Silver staining of Alzheimer's neurofibrillary changes by means of physical development. Acta Morphol. Acad. Sci. Hung. *19*, 1–8.

Geinisman, Y. (1979). Loss of axosomatic synapses in the dentate gyrus of aged rats. Brain Res. *168*, 485–492.

Geinisman, Y., Bondareff, W., and Dodge, J.T. (1977). Partial deafferentation of neurons in the dentate gyrus of the senescent rat. Brain Res. *134*, 541–545.

Gómez-Isla, T., Price, J.L., McKeel, D.W., Jr., Morris, J.C., Growdon, J.H., and Hyman, B.T. (1996). Profound loss of layer II entorhinal cortex neurons occurs in very mild Alzheimer's disease. J. Neurosci. *16*, 4491–4500.

Gossen, M., and Bujard, H. (1992). Tight control of gene expression in mammalian cells by tetracycline-responsive promoters. Proc. Natl. Acad. Sci. USA *89*, 5547–5551.

Harris, J.A., Devidze, N., Verret, L., Ho, K., Halabisky, B., Thwin, M.T., Kim, D., Hamto, P., Lo, I., Yu, G.Q., et al. (2010). Transsynaptic progression of amyloid-β-induced neuronal dysfunction within the entorhinal-hippocampal network. Neuron *68*, 428–441.

Hasegawa, M., Arai, T., Akiyama, H., Nonaka, T., Mori, H., Hashimoto, T., Yamazaki, M., and Oyanagi, K. (2007). TDP-43 is deposited in the Guam parkinsonism-dementia complex brains. Brain *130*, 1386–1394.

Hjorth-Simonsen, A., and Jeune, B. (1972). Origin and termination of the hippocampal perforant path in the rat studied by silver impregnation. J. Comp. Neurol. *144*, 215–232.

Hyman, B.T., and Trojanowski, J.Q. (1997). Consensus recommendations for the postmortem diagnosis of Alzheimer disease from the National Institute on Aging and the Reagan Institute Working Group on diagnostic criteria for the neuropathological assessment of Alzheimer disease. J. Neuropathol. Exp. Neurol. *56*, 1095–1097.

Hyman, B.T., Van Hoesen, G.W., Damasio, A.R., and Barnes, C.L. (1984). Alzheimer's disease: cell-specific pathology isolates the hippocampal formation. Science *225*, 1168–1170.

Hyman, B.T., Kromer, L.J., and Van Hoesen, G.W. (1987). Reinnervation of the hippocampal perforant pathway zone in Alzheimer's disease. Ann. Neurol. *21*, 259–267.

Hyman, B.T., Kromer, L.J., and Van Hoesen, G.W. (1988). A direct demonstration of the perforant pathway terminal zone in Alzheimer's disease using the monoclonal antibody Alz-50. Brain Res. *450*, 392–397.

Hyman, B.T., Van Hoesen, G.W., and Damasio, A.R. (1990). Memory-related neural systems in Alzheimer's disease: an anatomic study. Neurology *40*, 1721–1730.

Hyman, B.T., Gomez-Isla, T., and Irizarry, M.C. (1998). Stereology: a practical primer for neuropathology. J. Neuropathol. Exp. Neurol. *57*, 305–310.

Iliev, A.I., Ganesan, S., Bunt, G., and Wouters, F.S. (2006). Removal of pattern-breaking sequences in microtubule binding repeats produces instantaneous tau aggregation and toxicity. J. Biol. Chem. *281*, 37195–37204.

Irizarry, M.C., McNamara, M., Fedorchak, K., Hsiao, K., and Hyman, B.T. (1997). APPSw transgenic mice develop age-related A beta deposits and neuropil abnormalities, but no neuronal loss in CA1. J. Neuropathol. Exp. Neurol. *56*, 965–973.

Johnson, G.V., Seubert, P., Cox, T.M., Motter, R., Brown, J.P., and Galasko, D. (1997). The tau protein in human cerebrospinal fluid in Alzheimer's disease consists of proteolytically derived fragments. J. Neurochem. *68*, 430–433.

Koffie, R.M., Meyer-Luehmann, M., Hashimoto, T., Adams, K.W., Mielke, M.L., Garcia-Alloza, M., Micheva, K.D., Smith, S.J., Kim, M.L., Lee, V.M., et al. (2009). Oligomeric amyloid beta associates with postsynaptic densities and correlates with excitatory synapse loss near senile plaques. Proc. Natl. Acad. Sci. USA *106*, 4012–4017.

Micheva, K.D., and Smith, S.J. (2007). Array tomography: a new tool for imaging the molecular architecture and ultrastructure of neural circuits. Neuron *55*, 25–36.

Mocanu, M.M., Nissen, A., Eckermann, K., Khlistunova, I., Biernat, J., Drexler, D., Petrova, O., Schönig, K., Bujard, H., Mandelkow, E., et al. (2008). The potential for beta-structure in the repeat domain of tau protein determines aggregation, synaptic decay, neuronal loss, and coassembly with endogenous Tau in inducible mouse models of tauopathy. J. Neurosci. *28*, 737–748.

Nakano, I., Iwatsubo, T., Otsuka, N., Kamei, M., Matsumura, K., and Mannen, T. (1992). Paired helical filaments in astrocytes: electron microscopy and immunohistochemistry in a case of atypical Alzheimer's disease. Acta Neuropathol. *83*, 228–232.

Nishimura, M., Tomimoto, H., Suenaga, T., Namba, Y., Ikeda, K., Akiguchi, I., and Kimura, J. (1995). Immunocytochemical characterization of glial fibrillary tangles in Alzheimer's disease brain. Am. J. Pathol. *146*, 1052–1058.

Papasozomenos, S.C. (1989a). Tau protein immunoreactivity in dementia of the Alzheimer type. I. Morphology, evolution, distribution, and pathogenetic implications. Lab. Invest. *60*, 123–137.

Papasozomenos, S.C. (1989b). Tau protein immunoreactivity in dementia of the Alzheimer type: II. Electron microscopy and pathogenetic implications. Effects of fixation on the morphology of the Alzheimer's abnormal filaments. Lab. Invest. *60*, 375–389.

Price, S.R., De Marco Garcia, N.V., Ranscht, B., and Jessell, T.M. (2002). Regulation of motor neuron pool sorting by differential expression of type II cadherins. Cell *109*, 205–216.

Santacruz, K., Lewis, J., Spires, T., Paulson, J., Kotilinek, L., Ingelsson, M., Guimaraes, A., DeTure, M., Ramsden, M., McGowan, E., et al. (2005). Tau suppression in a neurodegenerative mouse model improves memory function. Science *309*, 476–481.

Schaeren-Wiemers, N., and Gerfin-Moser, A. (1993). A single protocol to detect transcripts of various types and expression levels in neural tissue and cultured cells: in situ hybridization using digoxigenin-labelled cRNA probes. Histochemistry *100*, 431–440.

Scheff, S.W., and Price, D.A. (2006). Alzheimer's disease-related alterations in synaptic density: neocortex and hippocampus. J. Alzheimers Dis. *9* (3, Suppl), 101–115.

Steward, O. (1976). Topographic organization of the projections from the entorhinal area to the hippocampal formation of the rat. J. Comp. Neurol. *167*, 285–314.

Sun, A., Nguyen, X.V., and Bing, G. (2002). Comparative analysis of an improved thioflavin-s stain, Gallyas silver stain, and immunohistochemistry for neurofibrillary tangle demonstration on the same sections. J. Histochem. Cytochem. *50*, 463–472.

Terry, R.D., Masliah, E., Salmon, D.P., Butters, N., DeTeresa, R., Hill, R., Hansen, L.A., and Katzman, R. (1991). Physical basis of cognitive alterations in Alzheimer's disease: synapse loss is the major correlate of cognitive impairment. Ann. Neurol. *30*, 572–580.

Tremblay, M.A., Acker, C.M., and Davies, P. (2010). Tau phosphorylated at tyrosine 394 is found in Alzheimer's disease tangles and can be a product of the Abl-related kinase, Arg. J. Alzheimers Dis. *19*, 721–733.

Tucker, K.L., Meyer, M., and Barde, Y.A. (2001). Neurotrophins are required for nerve growth during development. Nat. Neurosci. *4*, 29–37.

van Groen, T. (2001). Entorhinal cortex of the mouse: cytoarchitectonical organization. Hippocampus *11*, 397–407.

Van Hoesen, G., and Pandya, D.N. (1975). Some connections of the entorhinal (area 28) and perirhinal (area 35) cortices of the rhesus monkey. I. Temporal lobe afferents. Brain Res. *95*, 1–24.

Witter, M.P. (2007). The perforant path: projections from the entorhinal cortex to the dentate gyrus. Prog. Brain Res. *163*, 43–61.

Witter, M.P., Griffioen, A.W., Jorritsma-Byham, B., and Krijnen, J.L. (1988). Entorhinal projections to the hippocampal CA1 region in the rat: an underestimated pathway. Neurosci. Lett. *85*, 193–198.

Yasuda, M., and Mayford, M.R. (2006). CaMKII activation in the entorhinal cortex disrupts previously encoded spatial memory. Neuron *50*, 309–318.

Zhao, L., Ma, Q.L., Calon, F., Harris-White, M.E., Yang, F., Lim, G.P., Morihara, T., Ubeda, O.J., Ambegaokar, S., Hansen, J.E., et al. (2006). Role of p21-activated kinase pathway defects in the cognitive deficits of Alzheimer disease. Nat. Neurosci. *9*, 234–242.